Preclinical Dosimetry, Imaging, and Targeted Radionuclide Therapy Studies of Lu-177 Labeled Albumin-Binding, PSMA-Targeted CTT1403

Xiaoxi Ling[1], **Joseph D. Latoche**[1], **Cindy J. Choy**[2], **Brenda F. Kurland**[3], **Charles M. Laymon**[4,5], **Yijen Wu**[6,7], **Nathan Salamacha**[6,7], **Ding Shen**[1], **Jonathan J. Geruntho**[1], **Lora H. Rigatti**[8,9], **Hillarie P. Windish**[2], **Beatrice Langton-Webster**[2], **Clifford E. Berkman**[2], **Carolyn J. Anderson**[1,4,5,10,*]

[1.]Department of Medicine, University of Pittsburgh, Pittsburgh, PA

[2.]Cancer Targeted Technology, Woodinville, WA

[3.]Department of Biostatistics, University of Pittsburgh, Pittsburgh, PA

[4.]Department of Radiology, University of Pittsburgh, Pittsburgh, PA

[5.]Department of Bioengineering, University of Pittsburgh, Pittsburgh, PA

[6.]Department of Developmental Biology, University of Pittsburgh, Pittsburgh, PA

[7.]Rangos Research Center Animal Imaging Core, Children's Hospital of Pittsburgh of UPMC, Pittsburgh, PA

[8.]Division of Laboratory Animal Resources, University of Pittsburgh, Pittsburgh, PA

[9.]University of Pittsburgh Cancer Institute, University of Pittsburgh, Pittsburgh, PA

[10.]Department of Pharmacology & Chemical Biology, University of Pittsburgh, Pittsburgh, PA

Abstract

Purpose: Prostate-specific membrane antigen (PSMA) continues to be the hallmark biomarker for prostate cancer as it is expressed on nearly all prostatic tumors. In addition, increased PSMA expression correlates with castration resistance and progression to the metastatic stage of the disease. Recently, we combined both an albumin-binding motif and an irreversible PSMA inhibitor to develop the novel PSMA-targeted radiotherapeutic agent, CTT1403. This molecule was novel in the field of PSMA-targeted agents as its key motifs resulted in extended blood circulation time and tumor uptake, rapid and extensive internalization into PSMA+ cells, and promising therapeutic

*Corresponding Author Carolyn J. Anderson, PhD, Department of Medicine, University of Pittsburgh, 3501 Fifth Ave Room 10020, Pittsburgh, PA 15260, Phone: 412-624-6887, Fax: 412-648-6101, cja34@pitt.edu.

Conflict of Interest Statement

CJA is on the Scientific Advisory Board of Lumiphore (Berkeley, CA). XL, HW, BLW are currently employees of CTT. CEB serves a consultant to Cancer Targeted Technology and is the inventor of the CTT140X agents and the CTT1298 PSMA-inhibitor scaffold.

efficacy. The objective of this study was to perform IND-enabling translational studies on CTT1403 in rodent models.

Procedures: A dose optimization study was performed in PSMA+ tumor-bearing mice. Treatment groups were randomly selected to receive one to three 14 MBq injections of CTT1403. Control groups included: 1) saline; 2) non-radioactive [^{175}Lu]CTT1403; or 3) two injections of 14 MBq CTT1751, a Lu-177 labeled non-targeted radiolabeled albumin-binding moiety. Tumor growth was monitored up to 120 days. Small animal single photon emission tomography/x-ray computed tomography imaging was performed with CTT1403 and CTT1751 in PC3-PIP tumor-bearing mice to visualize infiltration of the Lu-177 labeled agent into the tumor. In preparation for a first-in-human study, human absorbed doses were estimated based on rat biodistribution out to 5 weeks to determine a safe CTT1403 therapy dose in humans.

Results: Two to 3 injections of 14 MBq CTT1403 yielded significant tumor growth inhibition and increased survival compared to all control groups and mice receiving 1 injection of 14 MBq CTT1403. Five of 12 mice receiving 2 or 3 injections of CTT1403 survived to the 120 days post-treatment study endpoint. Dosimetry identified the kidneys as the dose limiting organ, with an equivalent dose of 5.18 mSv/MBq, resulting in a planned maximum dose of 4.4 GBq for Phase 1 clinical trials.

Conclusions: The preclinical efficacy and dosimetry of CTT1403 suggest that this agent has significant potential to be safe and effective in humans.

Introduction

Prostate-specific membrane antigen (PSMA) continues to be the hallmark biomarker for prostate cancer as it is expressed on nearly all prostatic tumors. In addition, increased PSMA expression correlates with castration resistance and progression to the metastatic stage of the disease. Enormous effort has been dedicated towards PSMA as a diagnostic nuclear medicine imaging biomarker for prostate cancer [1–2]. Early efforts involved radiolabeled antibodies targeting PSMA, with the focus shifting from large PSMA antibodies to small-molecule based PSMA binding ligands [3]. Capromab pendetide, the first FDA-approved diagnostic agent for prostate cancer using single-photon emission computerized tomography (SPECT) imaging, is based on an In-111 labeled monoclonal anti-PSMA antibody 7E11 [4]. This agent binds an intracellular domain of PSMA that is not readily accessible to live prostate cancer cells, and for that reason has not been highly successful. The antibody J591 that binds the extracellular domain of PSMA, has been labeled with Zr-89 for imaging, with improved targeting over In-111 labeled 7E11 [5]. Ga-68 labeled PSMA-11, a small molecule positron emission tomography (PET) imaging agent, is currently in multiple Phase II and Phase III clinical trials for prostate cancer diagnosis [6].

Targeted radionuclide therapy agents incorporate energetic nuclides that decay by particle emission (alpha or beta particles, low energy electrons) as therapeutic payloads. The radionuclide is targeted to cancer cells through binding of an enzyme or receptor ligand to

its targeted protein [7]. The energetic particles damage DNA to disrupt cell growth. Lutetium-177 ($T_{1/2} = 6.7$ d; β^- (100%; $E_{max} = 498$ keV)) is a logical choice for targeted radionuclide therapy, as the lower energy beta particles have a mean range of 670 μm, allowing for successful eradication of tumors and metastatic sites while limiting damage to normal tissues [8] [^{177}Lu]PSMA-617 is a urea-based PSMA-targeted small-molecule that has shown impressive efficacy in castrate-resistant metastatic prostate cancer [9] and is currently in Phase III clinical trials in the US (NCT03511664).

A common feature of the radiolabeled small-molecule PSMA binding ligands is their rapid excretion via kidneys due to their highly charged nature, a feature which is critical for high affinity binding to PSMA [10]. While rapid clearance can be desirable from the diagnostic imaging perspective as it minimizes background signal, the resulting short circulation half-life limits the delivery window for therapeutic payloads to reach the target. Moreover, due to rapid clearance kinetics most of the payload does not reach the tumor, and the delivery of high doses of Lu-177 labeled therapeutic agents becomes expensive and wasteful. Therefore, alternative strategies to increase the circulation half-life of small molecules is needed.

We recently reported a new Lu-177 labeled PSMA targeted radiotherapeutic agent, CTT1403, that incorporates an albumin-binding motif to extend the blood circulation time of the irreversible PSMA inhibitor [11], ameliorating the rapid renal clearance pharmacokinetic profile that characterizes most PSMA targeting agents [11]. CTT1403 displayed markedly increased tumor uptake and tumor:background ratios in biodistribution studies and imparted dramatically improved survival of PSMA+ PC3-PIP tumor-bearing mice compared to animals treated with a PSMA compound that did not contain the albumin-binding moiety.

Given the promising efficacy of CTT1403 in PSMA+ tumor-bearing mice, this agent was further investigated in pre-clinical models in preparation for translation to first-in-human studies. Here we report results of the IND-enabling studies of CTT1403 in rodent models, including dosimetry, dose optimization, and SPECT imaging.

Materials and Methods

Unless otherwise specified, all reagents and solvents, in trace metal grade or HPLC grade whenever possible, were obtained from Sigma-Aldrich (St. Louis, MO) or Thermo Fisher (Pittsburgh, PA). Azido-mono-amide-DOTA (DOTA-Azide) was obtained from Macrocyclics (Plano, TX). Lutetium-177, in the form of [^{177}Lu]Lutetium Chloride in 0.05 M hydrochloric acid, was obtained from the National Isotope Development Center at Oak Ridge National Laboratory (Oak Ridge, TN).

Experiments on laboratory animals were performed in accordance with and approved by the University of Pittsburgh Institutional Animal Care and Use Committee (IACUC). All applicable institutional and/or national guidelines for the care and use of animals were followed. Male, athymic nude mice (NCr nude, 6–8 weeks) were purchased from Charles River Laboratories (Wilmington, MA). Mice were housed in groups of 3–4 in ventilated cages on hardwood chip bedding. Male, Sprague Dawley rats (226–250 g) were purchased from Charles River Laboratories. Rats were housed 2 per cage, with the exception of the 5

week group in the dosimetry study, which were housed individually in metabolism cages with additional enrichment. Food and water were provided *ad libitum*. Animals were acclimated for at least 72 h prior to any procedures.

Synthesis and Radiolabeling CTT1403 and CTT1751

The preparation of CTT1403 (developed by Cancer Targeted Technology) and its radiolabeling precursor CTT1402 was previously reported [11]. The process is briefly described in the Supporting Information. The preparation of non-radioactive [^{175}Lu]CTT1403 was similar to that of CTT1403 except for complexation of DOTA-azide with non-radioactive lutetium chloride. Lutetium-177 labeling of the DOTA-conjugated albumin binding moiety, CTT1751, was performed as done with CTT1403. The preparation of radiolabeling precursor CTT1750 is described in the Electronic Supplementary Information (ESM).

Cell line

The human prostate cancer cell line PC3-PIP (PSMA-positive) was obtained from Dr. Martin Pomper (Johns Hopkins University). As we previously described in Choy, *et al.* [11], cells were propagated in standard growth media (RPMI-1640 supplemented with 10% Fetal Bovine Serum (FBS), 100 units/ml Penicillin, and 100 μg/ml Streptomycin) in a humidified incubator at 37°C under 5% CO2. The cell line was passaged to around 70% confluence, with isolation performed using trypsin (0.25%, 0.1% EDTA) for 12–18 min.

Dose Optimization (efficacy)

The goal of this study was to optimize the dose and injection regimen of CTT1403 in the PC3-PIP mouse model, with survival as the primary endpoint. Three treatment groups received 1–3 injections of 14 MBq CTT1403 at 14-day intervals (Fig. 1a; Groups CTT1403×1, CTT1403×2, and CTT1403×3, respectively). This activity level was selected based on (1) demonstrated uptake and longevity of a 1.85 MBq CTT1403 injection in the previous biodistribution study (46.5 ± 14.5 %IA/g and 24.2 ± 4.2 %IA/g at 72 and 168 h post-injection, respectively) [11]; and (2) demonstrated tumor regression in the single injection efficacy study after 7–10 days after administration [11]. The three control groups received saline, [^{175}Lu]CTT1403, and non-PSMA targeting CTT1751.

Two separate cohorts of NCr nude male mice (15 and 24 mice, respectively) were injected with 3×10^5 PC3 (PSMA+) cells subcutaneously in the right shoulder 20 days (Cohort 1) or 19 days (Cohort 2) before administration of therapy. Animals with smaller tumors at baseline were assigned to control groups to decrease within-group variability in treatment groups and to protect against any failed xenografts. In each cohort on day 0, 3 mice were given saline and 3 mice were given [^{175}Lu]CTT1403 (0.88 nmole), 9 mice were given 14 MBq CTT1403 therapy (1.18–1.33 nmol, 10.5 – 11.9 MBq/nmol). On day 14, two-thirds of the mice receiving active CTT1403 therapy were selected to receive a second injection using 2:1 block-randomization following ranking based in the most recent tumor volume. On day 28, the same process used 1:1 block randomization to select half of the remaining animals to receive a third injection. CTT1751 therapy (6 mice) was conducted only in Cohort 2; 14 MBq of CTT1751 (1.2 nmol, 11.9 Mbq/nmol) was given on day 0 and day 14.

Body weights and tumor volumes were measured before the injection and three times per week post injection. The tumor volume (V) was determined according to the equation [V = $(\pi \div 6) \times L \times W \times H$], where L is the longest axis and W is the perpendicular axis to L, and H is the perpendicular axis to L and W plane. Tumor volume doubling time was assessed by a random intercept model (by animal), with a fixed cohort effect. Growth rates among the 6 treatment groups were compared as estimated marginal means of linear trends [12], with Tukey-Kramer adjustment for pairwise comparisons. Endpoint (sacrifice) criteria were defined as when the longest axis of measurement of tumor exceeded 1.5 cm, there was active ulceration of the tumor, 20% body weight loss, or 120 days post administration. Survival curves from date of tumor implant were described by the Kaplan-Meier method, with group comparisons by the log-rank test.

SPECT imaging

SPECT imaging was performed for visualization of CTT1403 infiltration into tumor and non-target tissues as a proof of concept for potential human dose estimation, and compared to results from the terminal biodistribution studies previously reported. Nine NCr nude male mice were injected with 3×10^5 PC3-PIP (PSMA+) cells subcutaneously in the right shoulder 24 days before start of the study with CTT1403 or CTT1751. Initial tumor sizes were approximately 200 – 450 mm^3. Seven mice were injected with 28 MBq CTT1403 (2.36 nmol, 11.9 MBq/nmol) via tail vein and two mice were injected with 28 MBq CTT1751 (2.36 nmol, 11.9 MBq/nmol). SPECT/x-ray computed tomography (CT) images were collected 4, 24, 48, 72, and 168 h post-injection using a Siemens Inveon SPECT/PET/CT scanner. A "phantom" tube as fiducial marker containing half of injected activity (14 MBq) was placed on the right side of the tail for signal calibration. All animals enrolled in the study were euthanized after the last imaging time point.

Images were generated using IRW software (Siemens). Image analysis was performed using VivoQuant (InviCRO; Boston, MA). Regions of interest (ROI) were defined around key organs and tissues, based on corresponding CT or SPECT signals. CTT1403 decay corrected activity uptake (%IA/organ) was calculated using the following equation, whereas the mean counts and volume were based on ROI analysis.

$$\%IA/Organ = \left(\frac{Mean\ Counts_{ROI} \times Volume_{ROI}}{Mean\ Counts_{Phantom} \times Volume_{Phantom} \times 2} \right)$$

Bone and muscle uptake were adjusted by a factor calculated based on the product of volume of the ROI and tissue density (2.167 g/ml for bone [13] and 1.000 g/ml for muscle) to the weight of the corresponding tissue using the product of whole body weight and a factor (0.109 for bone and 0.410 for muscle). The tumor to background ratio was calculated using the mean voxel value of tumor ROI divided by the corresponding value of the background organ or tissue.

Dosimetry

The study was performed in two separate cohorts of Sprague Dawley male rats. In the first cohort, thirty rats were injected intravenously with 13 MBq CTT1403 (10.8 nmol, 1.2 MBq/nmol) via the tail vein. Animals were humanely sacrificed, and tissues harvested at 1 h, 6 h, 1 d, 2 d, 1 week (wk) and 2 wk post-injection. In the second cohort, ten rats were injected intravenously with 18 MBq CTT1403 (19.6 nmol, 0.91 MBq/nmol) tracer via the tail vein. The increased injection activities at the later time points were necessary to ensure reliable quantification due to low counts in tissues after several half-lives of decay. Five rats were housed in normal cages for 3 weeks. The other five rats were housed in individual metabolic cages for 5 weeks for assessment of excretion. Urine and feces samples from these animals were collected at 6 h, 1 d, 2 d, and 1 wk post-injection. After 1 week, urine and feces samples were collected every other day up to 5 weeks post-injection. Samples from the same animal were combined and grouped at 2, 3, and 5 wk post injection. Animals were euthanized, and tissues harvested 3 and 5 wk post-injection, respectively.

Exposure to CTT1403 was assessed in adrenals, bladder, blood, bone, brain, fat, heart, kidneys, liver, lungs, marrow, muscle, pancreas, pituitary, prostate, small intestine, spleen, stomach, testes, thymus, thyroid, lower large intestine, upper large intestine, lacrimal glands, and salivary glands. All tissues as well as urine and feces were counted in a gamma counter. All organs were harvested intact except for the following, which were collected as partial organs and corrected based on percentage of body weight: blood (7%), bone (10.9%), fat (13.8%), bone marrow (3%), and muscle (41%). Tissue weights and counts per minute (CPM) were used to complete a biodistribution worksheet for calculation. Urine and feces samples counts were used for excretion calculation.

Activity measured for each organ was multiplied by a factor, f [14].

$$f = \frac{m_{human}/M_{human}}{m_{rat}/M_{rat}}$$

where m_{rat} and m_{human} are rat and human organ mass respectively, and M_{rat} and M_{human} are rat and human total body mass respectively. Thus, f accounts for the difference in fraction of body mass for each organ between rat and human. Most human weights were taken from the human male model incorporated in the widely used dosimetry program OLINDA/EXM 1.0 [15].

Scaled organ activities for each time point were divided by injected activity and averaged over the 5 rats. The averaged values were integrated over time using the trapezoidal method to yield human residence times for each organ. Human bone residence times were subdivided into cortical-bone and trabecular-bone components by assuming bone activity partitioned according to the relative masses of the two bone types. Blood and fat are not OLINDA/EXM 1.0 source organs. The residence time for these components was not scaled (f, above) and were combined and entered as a "remainder" source, i.e. spread uniformly throughout the body. The residence times were used as input to OLINDA/EXM 1.0, which was used to calculate equivalent dose to the various target organs and the whole body.

The lacrimal and salivary glands are of particular interest for assessment of CTT1403 dosimetry, as they may be dose-limiting for other PSMA-targeted therapeutic agents [16], but are not specifically included within OLINDA/EXM 1.0. A sphere model in OLINDA/EXM 1.0 was used [16–18] to model these glands. Prostate dose was calculated using a prostate model in OLINDA/EXM 1.0.

Results

Dose optimization (efficacy)

In the prior CTT1403 therapeutic efficacy study in the PC3-PIP mouse prostate tumor model, 28 MBq CTT1403 treatment was administered 10 days after tumor cell implantation; in this group of mice 90% survived 120 days compared to controls with a median survival of 42 days [11]. In the current study, treatment commenced in animals with more advanced tumors, however, this also led to greater variability in tumor size at the start of treatment (Fig. 1b). Mice with the smallest tumors were assigned to the control groups (saline, [^{175}Lu]CTT1403 or CTT1751). There was no growth inhibition in any of the control groups (Fig. 2a); estimated tumor volume doubling time was 4.5–5.7 days and did not differ among the 3 groups (Tukey-adjusted $p > 0.35$) (Fig. 2a and b). For all CTT1403 treatment groups, the injection activity was reduced by half to 14 MBq in order to determine if fractionating the dose would be as effective as a single 28 MBq dose as previously published [11]. The fractionation schedule was based on demonstrated tumor regression in the single injection efficacy study after 7–10 days after administration. Tumor regression was observed 7–10 days post-treatment, similar to what was reported for single injection treatment [11]. After a single injection of 14 MBq CTT1403 (CTT1403×1, Fig. 2b and c), tumors began to grow again after a brief period of regression, while after 2 or 3 injections of CTT1403 (CTT1403×2 and CTT1403×3; Fig. 2b and c) growth was markedly inhibited. Three of 6 animals receiving 2 injections, and 2 of 6 animals receiving 3 injections of CTT1403, had persistent tumor regression and survived through the planned termination date (120 days post-treatment). One other mouse in the CTT1403×2 group started CTT1403 therapy with a 581 mm^3 tumor that grew to 713 mm^3 (day 9) then shrunk to 153 mm^3 by day 37 (following 2 injections of CTT1403), before rebounding. Another mouse in the CTT1403×3 group exhibited a >99% decrease in tumor size from 474 mm^3 at day 5 to 3 mm^3 by day 49, again followed by a rebound. Two and 3 injections of CTT1403 conferred significant efficacy, mirroring results in the previous report [11] in which a single larger injection of 29 MBq was administered.

Survival post-tumor implantation is shown in Fig. 2d. Based on the tumor growth results (Fig. 2a), control groups were merged for group comparisons. The median survival for the control groups was 45 days (95% confidence interval (CI) 39–48 days); the CTT1403×1 median survival of 51.5 days (95% CI 4–71) trended towards being longer than controls but was shorter than for either CTT1403×2 (81 days, 75-N/A) or CTT1403×3 (112.5 days, 97-N/A) (see Table 1 for log-rank test results). Three injections of 14 MBq CTT1403 did not yield a statistically significant survival advantage over 2 injections (CTT1403×2 vs. CTT1403×3; p=0.961). Neither CTT1751, the untargeted Lu-177 labeled albumin-binding moiety, nor non-radioactive [^{175}Lu]CTT1403 reduced tumor burden or extended animal

survival (Fig. 2a and d), suggesting both the PSMA-targeting moiety and Lu-177 are essential for its therapeutic function.

SPECT imaging

Figure 3 shows representative serial images from PSMA-tumor bearing mice injected with CTT1403 (top) or CTT1751, which incorporates Lu-177 and the albumin binding moiety, but not the PSMA-targeting agent (bottom). Lutetium-177 emission was quantified by ROI analysis using VivoQuant and mean values are presented.

Tumor uptake of CTT1403 gradually increased over time, reaching a maximum at 48–72 h post-injection (10.7 ± 3.5 % injected activity (IA)/organ and 10.1 ± 2.8 %IA/organ, respectively) before gradually decreasing (4.7 ± 1.9 %IA/organ) after 168 h, comparable to the previous biodistribution study (Fig. 4a and Suppl. Fig. 1, see ESM). Kidney uptake peaked immediately after injection (14.5 ± 2.5 %IA/organ) and gradually decreased over the course of the study (2.9 ± 0.5 %IA/organ after 168 h). Heart uptake (blood pool) also peaked 4 h post-injection (5.6 ± 0.7 %IA/organ) and decreased significantly over the course of the study (<1 %IA/organ after 48 h). Bone and muscle uptake showed a similar clearance pattern. It should be noted that signal:noise and other artifacts may have interfered with detection of bone and muscle uptake due to the proximity of the ROI and the phantom tube, especially during the early time points.

Without PSMA targeting, CTT1751 exhibited low tumor uptake (0.8 and 1.4 %IA/organ for the two tested animals after 4 h) and declined rapidly thereafter (Fig. 4b). The time course of CTT1751 tumor uptake was similar to that of bone and muscle, reflective of the lack of specificity, and demonstrating the necessity of the PSMA-targeting motif. Blood pool uptake for CTT1751 (4.3 and 5.0 %IA/organ after 4 h, 1.8 and 2.0 %IA/organ after 48 h) was comparable to that observed for CTT1403, validating the impact of the albumin-binding moiety in slowing blood clearance.

The ratio of CTT1403 tumor uptake to blood pool increased over time, whereas it remained stable in the CTT1751 group (Fig. 4c), demonstrating target-specific tumor accumulation of CTT1403. Greater accumulation of CTT1403 compared to CTT1751 in kidney is likely due to elevated PSMA expression in rodent kidneys. The tumor:background ratios showed that while CTT1403 is cleared from blood, bone and muscle, it preferentially accumulates and remains within the tumor.

Dosimetry

In this study, the dosimetry of CTT1403 was determined in normal Sprague Dawley rats based on its biodistribution and excretion (Suppl. Fig. 3, see ESM). Time-activity curves of CTT1403 in blood, muscle, kidney, liver, salivary and lacrimal glands, show the kidney to have the highest uptake, with relatively low activity in the salivary and lacrimal glands (Fig. 5). CTT1403 cleared slowly from the blood over the first 2 days (from ~30 to ~5 %IA/ organ) and was cleared from the circulation almost completely after 1 week (<0.1 %IA/ organ). Non-PSMA expressing, highly vascularized organs such as muscle, lung, pancreas, and spleen had low CTT1403 uptake. Greater and more sustained uptake was observed in kidney, which increased over time during the first 2 days (up to 22 %IA/organ) and slowly

cleared over 3 weeks, due to PSMA expression known to be present in the mouse [19]. Minimal uptake was observed throughout the study in the gastrointestinal tract and glands of interest, including lacrimal and salivary glands. CTT1403 activity was detected in the urine and feces up to 3 weeks post-injection. Most of the radioactivity was cleared by 5 weeks post-injection (combined 66.9 ± 5.0 %IA were found in urine and feces samples).

Human residence times (disintegrations per injected activity) derived from rat time-activity curves and used for the dosimetry calculations are listed in Suppl. Table 1 (see ESM). The organ with the highest residence time was found to be the kidneys (17.9 h) followed by the remainder term (12.8 h), which as described in the Materials and Methods section, comprise blood and fat activity. Each of the other source organs had residence times of less than 10 h.

Human dosimetry results, derived from the residence times using OLINDA/EXM 1.0 are summarized in Table 2, which shows equivalent dose per injected activity (total column) as well as the equivalent dose contributions from beta and photon radiation. Also listed are effective dose equivalent (EDE) and effective dose (ED) along with individual organ contributions to each of these. The values for prostate, lacrimal, and salivary glands were calculated separately as described above and are listed at the end of the table. A whole-body equivalent dose of 0.0592 was found. The organ with the highest equivalent dose (5.19 mSv/ MBq) was the kidneys, followed by the osteogenic cells (0.177 mSv/MBq), adrenals (0.119 mSv/MBq), lacrimal gland (0.119 mSv/MBq) and the lungs (0.103 mSv/MBq). The calculated equivalent dose to all other individual organs was less than 0.1 mSv/MBq.

Discussion

Our previous study demonstrated for the first time that the addition of an albumin-binding motif to a Lu-177 labeled small-molecule PSMA inhibitor (CTT1403) greatly enhanced its pharmacokinetic performance by extending tumor residence time [11]. This key modification resolved the issue of rapid renal clearance observed for the previously published urea-based PSMA-targeted small-molecule agents, resulting in 14-fold higher maximum tumor uptake, improved tumor:kidney ratios (from 0.2–0.4 to 0.7–1), and most importantly, superior therapeutic efficacy compared to the same agent without an albumin binding moiety (CTT1401). Subsequent to the publication of CTT1403, incorporation of an albumin binding motif has been adopted by other groups and has been shown to confer similar favorable properties [20–24].

The objective of the current study was to perform pre-clinical IND-enabling studies to estimate safe doses of CTT1403 for first-in-human studies. We previously showed that a single injection of CTT1403 (29 MBq) reduced tumor burden and increased survival in PSMA+ tumor-bearing mice. A dose regimen consisting of fractionated or multiple lower dose administrations is a common strategy to maximize efficacy while minimizing toxicity to normal tissues [25]. We determined the efficacy of fractionated injections of CTT1403 in the therapeutic treatment of PSMA+ mouse tumors. Tumor growth inhibition was observed in all groups treated with CTT1403 starting around 7–10 days post administration compared to controls animals, where tumors grew continuously. Tumor burden in mice receiving 2–3 injections of CTT1403 was significantly reduced, with nearly half the mice surviving out to

120 days with no observable tumors. Fourteen MBq CTT1403 is equivalent to a human dose of approximately 2.7 GBq CTT1403 in a 70 kg adult, which is significantly less than the multiple injection regimen of 7.4 GBq currently in use for [^{177}Lu]PSMA-617 clinical trials (NCT03511664).

In addition to emitting beta particles for therapy, Lu-177 also emits gamma photons of suitable energy for SPECT imaging, which allows real time *in vivo* imaging of the biodistribution of Lu-177 labeled radiotherapeutic agents for estimation of dosimetry. This strategy is planned for the first-in-human clinical trial to estimate human dosimetry to better understand both exposure to normal tissues and dose to tumors. In this study, CTT1403 uptake in tumor and non-specific tissues based on SPECT/CT imaging showed a similar pattern to previous biodistribution results (Suppl. Fig. 1a, see ESM), aside from apparent increased kidney clearance in the SPECT study (Suppl. Fig. 1b, see ESM). A possible explanation for the discrepancy in kidney uptake and clearance of CTT1403 from SPECT imaging vs biodistribution is that the administered mass of CTT1403 was approximately 3.5 times higher in the SPECT imaging study (11.9 MBq/nmol in SPECT imaging study vs 2.74 – 3.04 MBq/nmol in previous biodistribution study).

To estimate the radioactive dose to normal human tissues, we used normal rats as a model to aid in selection of human doses of CTT1403 for the first-in-human Phase 1 clinical study. Kidney is the dose limiting organ with an equivalent dose of 5.18 mSv/MBq, which recommends a first in human administration of 4.4 GBq CTT1403 based on a conservative maximum kidney exposure of 23 Gy [26–30]; however, it should be noted that kidney radiation exposures of up to 40 Gy have been deemed safe for patients without renal risk factors [31]. Additionally, rodent kidneys are known to have significantly higher PSMA expression levels than human kidneys [19]. Given rodent overexpression, reduced kidney exposure is expected to be observed in the human clinical trial, reducing predicted cumulative kidney exposure after multiple administrations of CTT1403.

Of interest, the equivalent dose found for the red marrow, an organ of concern for radiation toxicity, was found to be 0.0548 mSv/MBq, which is relatively low compared to some other prostate therapy agents. For example, in a biodistribution study of ^{177}Lu-labeled J591 antibody, an absorbed dose of 0.32 mGy/MBq (which corresponds to an equivalent dose of 0.32 mSv/MBq) was reported [32] based on blood samples, which is substantially greater than that found in the current study.

Human dosimetry showed that about 50% and 70% of [^{177}Lu]PSMA-617 was excreted at 4 h and 12 h post administration, respectively [33]. In the study presented here, less than 15% of injected CTT1403 activity was excreted from normal rats after 1 d, and ~50% of injected activity was excreted after 1 week. A single 29 MBq therapeutic activity of CTT1403 to mice, which extended survival to beyond 120 days post-tumor administration, showed no overt signs of imparting toxicity [11]. Mice given up to three injections of 14 MBq CTT1403 over 4 weeks also survived for over 120 days with no signs of toxicity. Given this favorable clearance profile, agents such as CTT1403 that contain an albumin-binding moiety are expected to achieve similar therapeutic efficacy using significantly less radiolabeled agent than their non-albumin-binding counterparts.

Zan,g et al. recently reported a first-in-human study of [^{177}Lu]-EB-PSMA-617, where EB is Evans Blue dye, which is another albumin-binding moiety [34]. They reported the effective dose equivalent for [^{177}Lu]-EB-PSMA-617 was higher than that of [^{177}Lu]PSMA-617 (0.1294 ± 0.0395 mSv/MBq vs 0.0235 ± 0.0029 mSv/MBq, while the kidney dose was 2.39 ± 0.69 mSv/MBq compared to 0.39 ± 0.06 mSv/MBq for PSMA-617. The effective dose equivalent for CTT1403 based on rodent biodistribution is 0.385 mSv/MBq, with the kidney dose being 5.18 mSv/MBq. While the true benefits of an agent like CTT1403 or [^{177}Lu]DOTA-EB-PSMA-617 will depend on further in-depth human trials, we can hypothesize that administering less Lu-177 labeled agent has the potential to reduce toxicity and side effects to the patients while offering similar therapeutic outcomes, providing new strategies to protect off-target organs. It will also reduce external radiation exposure to hospital personnel and patients' families. Lastly, the cost of each treatment dose is expected to be less, as the radionuclides are some of the most expensive component of a radionuclide therapy.

Conclusions

Preclinical studies for CTT1403 in rodent models provide data demonstrating that this agent has strong potential for efficacy in humans at doses as low as 2.7 GBq. Dosimetry and toxicity studies in a normal rat model show the kidneys to be the dose-limiting organ, with an administration limit in humans of 4.4 GBq. Data reported here support the IND for clinical trial NCT03822871, a phase 1 dose escalation/dose expansion study evaluating the safety and efficacy of CTT1403 in patients with progressive metastatic castration-resistant prostate cancer (mCRPC).

Supplementary Material

Refer to Web version on PubMed Central for supplementary material.

Acknowledgements

References

1. von Eyben FE, Baumann GS, Baum RP (2018) PSMA diagnostics and treatments of prostate cancer become mature. Clin Trans Imag 6:145–148.

2. Zschaeck S, Lohaus F, Beck M, et al. (2018) PSMA-PET based radiotherapy: a review of initial experiences, survey on current practice and future perspectives. Radiat Oncol 13:90. [PubMed: 29751842]

3. Huang SS, Heston WDW (2017) Should Low Molecular Weight PSMA Targeted Ligands Get Bigger and Use Albumin Ligands for PSMA Targeting? Theranostics 7:1940–1941. [PubMed: 28638479]

4. Wynant GE, Murphy GP, Horoszewicz JS, et al. (1991) Immunoscintigraphy of prostatic cancer: preliminary results with ^{111}In-labeled monoclonal antibody 7E11-C5.3 (CYT-356). The Prostate 18:229–241. [PubMed: 2020619]

5. Pandit-Taskar N, O'Donoghue JA, Durack JC, et al. (2015) A Phase I/II Study for Analytic Validation of [89]Zr-J591 ImmunoPET as a Molecular Imaging Agent for Metastatic Prostate Cancer. Clin Cancer Res 21:5277–5285. [PubMed: 26175541]

6. Koerber SA, Utzinger MT, Kratochwil C, et al. (2017) ^{68}Ga-PSMA-11 PET/CT in Newly Diagnosed Carcinoma of the Prostate: Correlation of Intraprostatic PSMA Uptake with Several Clinical Parameters. J Nucl Med 58:1943–1948. [PubMed: 28619734]

7. Gallivanone F, Valente M, Savi A, et al. (2017) Targeted radionuclide therapy: frontiers in theranostics. Front Biosci 22:1750–1759.

8. Dash A, Pillai MR, Knapp FF Jr. (2015) Production of ^{177}Lu for Targeted Radionuclide Therapy: Available Options. Nucl Med Mol Imag 49:85–107.

9. Rahbar K, Ahmadzadehfar H, Kratochwil C, et al. (2017) German Multicenter Study Investigating ^{177}Lu-PSMA-617 Radioligand Therapy in Advanced Prostate Cancer Patients. J Nucl Med 58:85–90. [PubMed: 27765862]

10. Pillai MRA, Nanabala R, Joy A, et al. (2016) Radiolabeled enzyme inhibitors and binding agents targeting PSMA: Effective theranostic tools for imaging and therapy of prostate cancer. Nucl Med Biol 43:692–720. [PubMed: 27589333]

11. Choy CJ, Ling X, Geruntho JJ, et al. (2017) 177Lu-Labeled Phosphoramidate-Based PSMA Inhibitors: The Effect of an Albumin Binder on Biodistribution and Therapeutic Efficacy in Prostate Tumor-Bearing Mice. Theranostics 7:1928–1939. [PubMed: 28638478]

12. Lenth R Esimated Marginal Means, aka Least-Square Means. https://CRAN.R-project.org/package=emmeans.

13. Cory E, Nazarian A, Entezari V, et al. (2010) Compressive axial mechanical properties of rat bone as functions of bone volume fraction, apparent density and micro-ct based mineral density. J Biomech 43:953–960. [PubMed: 20003979]

14. Kirschner AS, Ice RD, Beierwaltes WH (1975) Radiation-Dosimetry of I-131–19-Iodocholesterol - Pitfalls of Using Tissue Concentration Data - Reply. J Nucl Med 16:248–249.

15. Stabin MG, Sparks RB, Crowe E (2005) OLINDA/EXM: The second-generation personal computer software for internal dose assessment in nuclear medicine. J Nucl Med 46:1023–1027. [PubMed: 15937315]

16. Hohberg M, Eschner W, Schmidt M, et al. (2016) Lacrimal Glands May Represent Organs at Risk for Radionuclide Therapy of Prostate Cancer with [177Lu]DKFZ-PSMA-617. Mol Imag Biol 18:437–445.

17. Yadav MP, Ballal S, Tripathi M, et al. (2017) Post-therapeutic dosimetry of ^{177}Lu-DKFZ-PSMA-617 in the treatment of patients with metastatic castration-resistant prostate cancer. Nucl Med Commun 38:91–98. [PubMed: 27782913]

18. Zechmann CM, Afshar-Oromieh A, Armor T, et al. (2014) Radiation dosimetry and first therapy results with a 124I/ 131I-labeled small molecule (MIP-1095) targeting PSMA for prostate cancer therapy. Eur J Nucl Med Mol Imaging 41:1280–1292. [PubMed: 24577951]

19. Aggarwal S, Ricklis RM, Williams SA, Denmeade SR (2006) Comparative study of PSMA expression in the prostate of mouse, dog, monkey, and human. The Prostate 66:903–910. [PubMed: 16496413]

20. Benesova M, Umbricht CA, Schibli R, Muller C (2018) Albumin-Binding PSMA Ligands: Optimization of the Tissue Distribution Profile. Mol Pharm 15:934–946. [PubMed: 29400475]

21. Kelly J, Amor-Coarasa A, Ponnala S, et al. (2018) Trifunctional PSMA-targeting constructs for prostate cancer with unprecedented localization to LNCaP tumors. Eur J Nucl Med Mol Imaging 45:1841–1851. [PubMed: 29623376]

22. Kuo HT, Merkens H, Zhang Z, et al. (2018) Enhancing Treatment Efficacy of ^{177}Lu-PSMA-617 with the Conjugation of an Albumin-Binding Motif: Preclinical Dosimetry and Endoradiotherapy Studies. Mol Pharm:5183–5191. [PubMed: 30251544]

23. Umbricht CA, Benesova M, Schibli R, Muller C (2018) Preclinical Development of Novel PSMA-Targeting Radioligands: Modulation of Albumin-Binding Properties To Improve Prostate Cancer Therapy. Mol Pharm 15:2297–2306. [PubMed: 29684274]

24. Wang Z, Tian R, Niu G, et al. (2018) Single Low-Dose Injection of Evans Blue Modified PSMA-617 Radioligand Therapy Eliminates Prostate-Specific Membrane Antigen Positive Tumors. Bioconjug Chem 29:3213–3221. [PubMed: 30105912]

25. Shargel L, Wu-Pong S, Yu ABC (2012) Chapter 8. Multiple-Dosage Regimens In Applied Biopharmaceutics & Pharmacokinetics. New York, NY: The McGraw-Hill Companies.

26. Emami B, Lyman J, Brown A, et al. (1991) Tolerance of normal tissue to therapeutic irradiation. Int J Radiat Oncol Biol Phys 21:109–122. [PubMed: 2032882]

27. Loke KSH, Padhy AK, et al. (2011) Dosimetric Considerations in Radioimmunotherapy and Systemic Radionuclide Therapies: A Review. World J Nucl Med 10:122–138. [PubMed: 22144871]

28. Delker A, Fendler WP, Kratochwil C, et al. (2016) Dosimetry for Lu-177-DKFZ-PSMA-617: a new radiopharmaceutical for the treatment of metastatic prostate cancer. Eur J Nucl Med Mol Imaging 43:42–51. [PubMed: 26318602]

29. Ilan E, Sandstrom M, Wassberg C, et al. (2015) Dose response of pancreatic neuroendocrine tumors treated with peptide receptor radionuclide therapy using ^{177}Lu-DOTATATE. J Nucl Med 56:177–182. [PubMed: 25593115]

30. Garske-Roman U, Sandstrom M, Fross Baron K, et al. (2018) Prospective observational study of 177Lu-DOTA-octreotate therapy in 200 patients with advanced metastasized neuroendocrine tumours (NETs): feasibility and impact of a dosimetry-guided study protocol on outcome and toxicity. Eur J Nucl Med Mol Imaging 45:970–988. [PubMed: 29497803]

31. Bodei L, Cremonesi M, Ferrari M, et al. (2008) Long-term evaluation of renal toxicity after peptide receptor radionuclide therapy with ^{90}Y-DOTATOC and ^{177}Lu-DOTATATE: the role of associated risk factors. Eur J Nucl Med Mol Imaging 35:1847–1856. [PubMed: 18427807]

32. Vallabhajosula S, Kuji I, Hamacher KA, et al. (2005) Pharmacokinetics and biodistribution of In-111-Lu-177-labeled J591 antibody specific for prostate-specific membrane antigen: Prediction of Y-90-J591 radiation dosimetry based on In-111 or Lu-177? J Nucl Med 46:634–641. [PubMed: 15809486]

33. Kurth J, Krause BJ, Schwarzenbock SM, Stegger L, Schafers M, Rahbar K (2018) External radiation exposure, excretion, and effective half-life in ^{177}Lu-PSMA-targeted therapies. EJNMMI Res 8:32. [PubMed: 29651569]

34. Zang J, Fan X, Wang H, et al. (2019) First-in-human study of ^{177}Lu-EB-PSMA-617 in patients with metastatic castration-resistant prostate cancer. Eur J Nucl Med Mol Imaging 46:148–158. [PubMed: 30090965]

35. Kramer CY (1956) Extension of Multiple Range Tests to Group Means with Unequal Numbers of Replications. Biometrics 12:307–310.
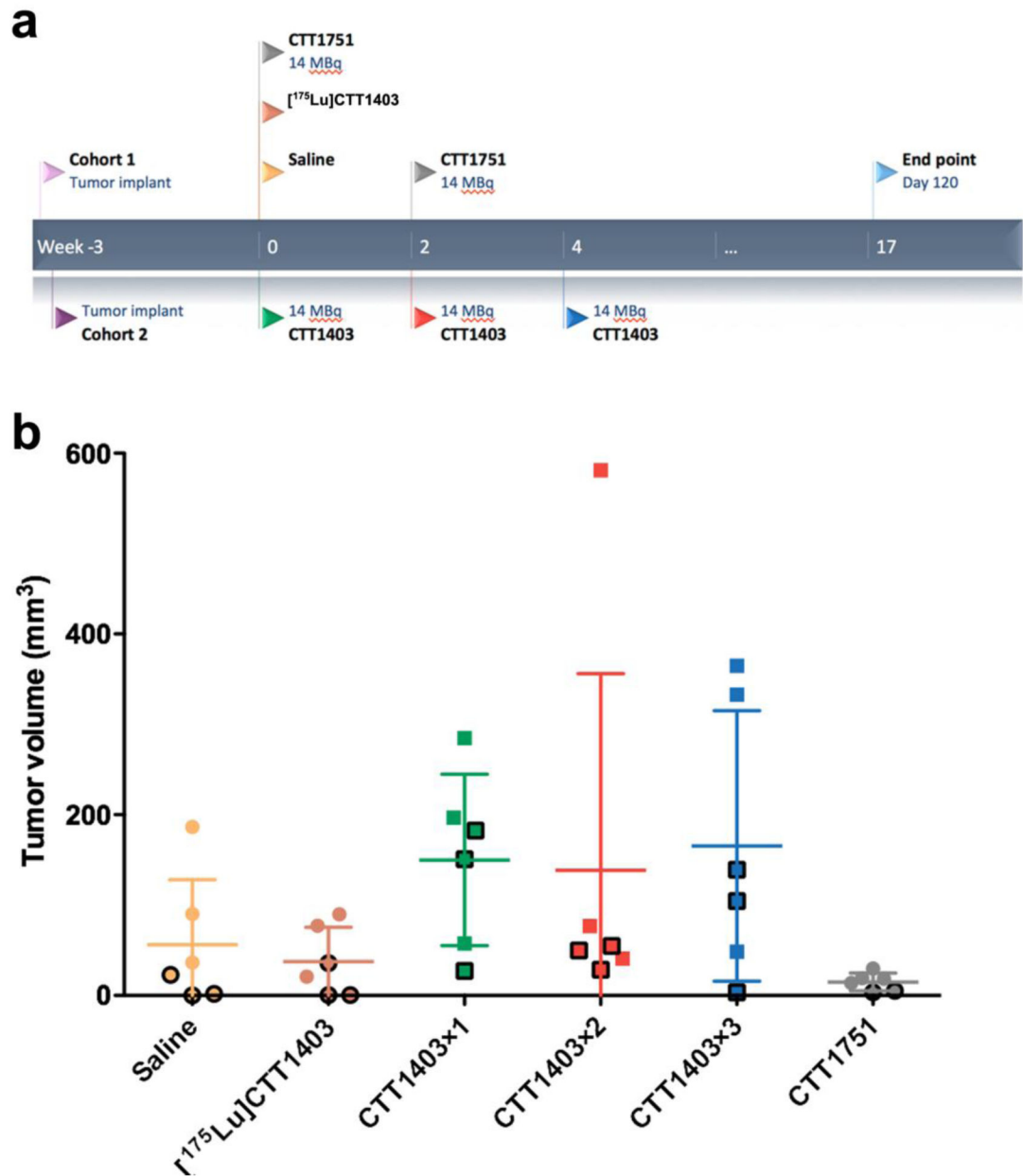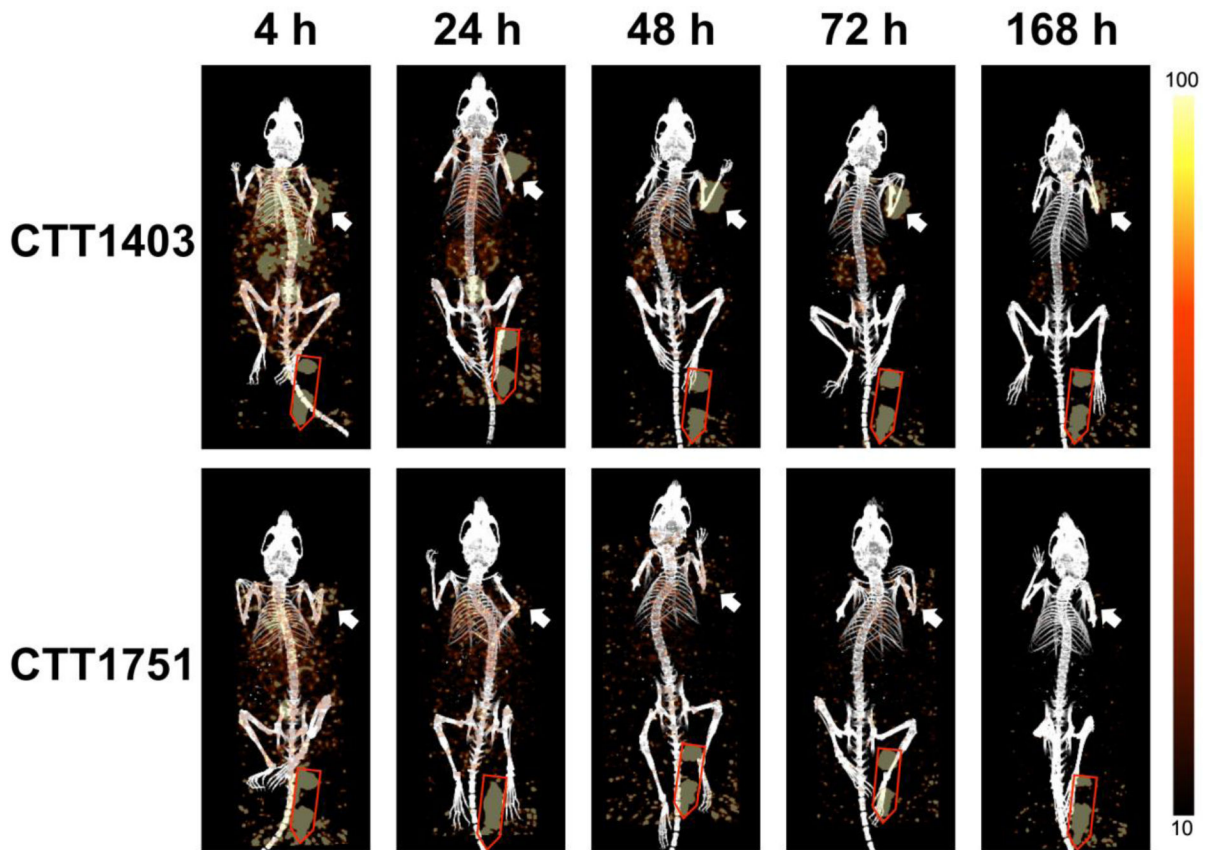
Figure 1.
Schematic of dose optimization study. **a** Experiment design; **b** Tumor size distribution at the start of treatment, black outlines indicate animals that survived longer than the median survival.
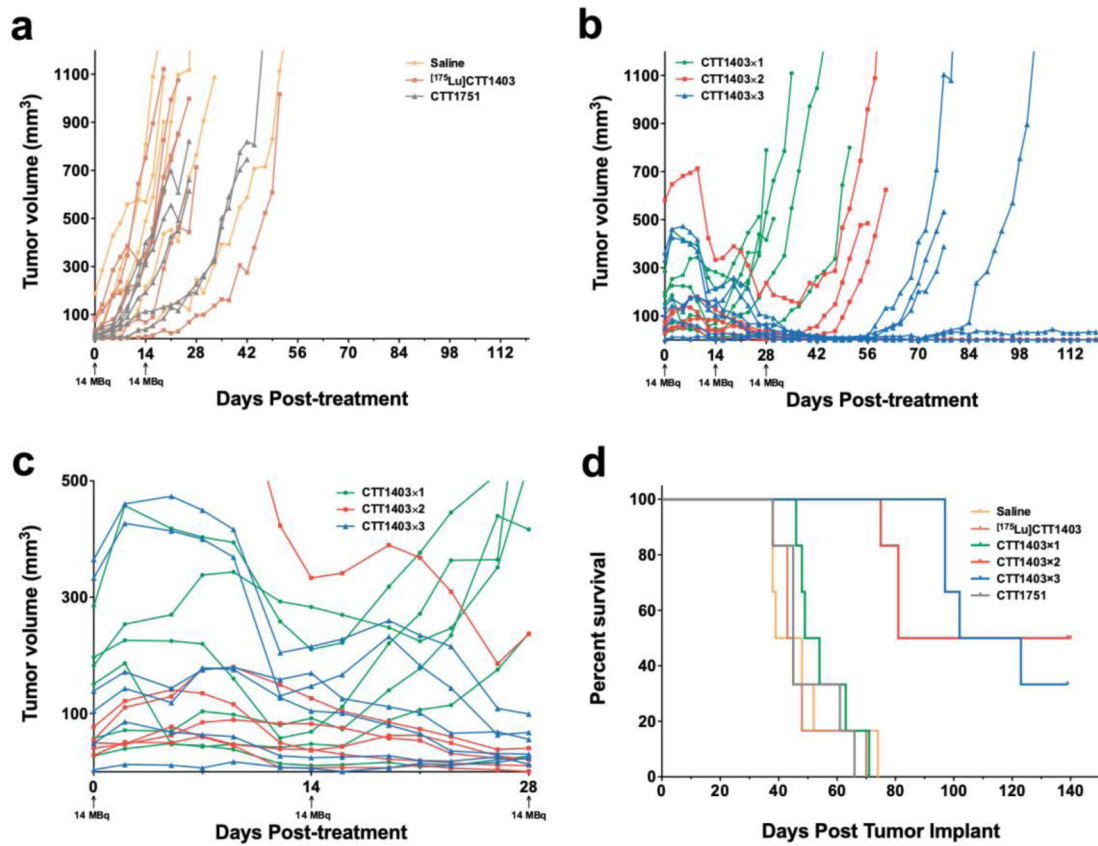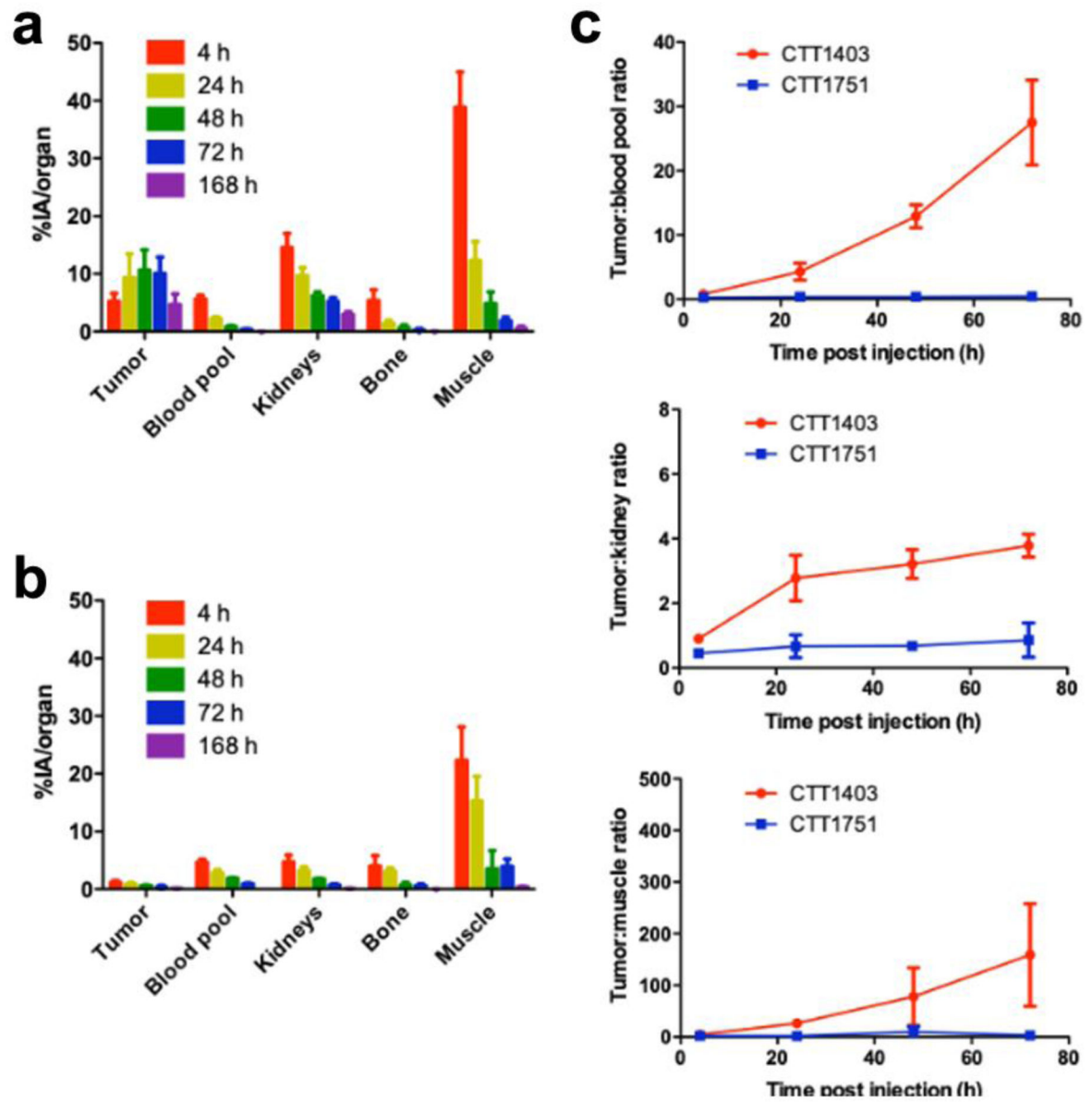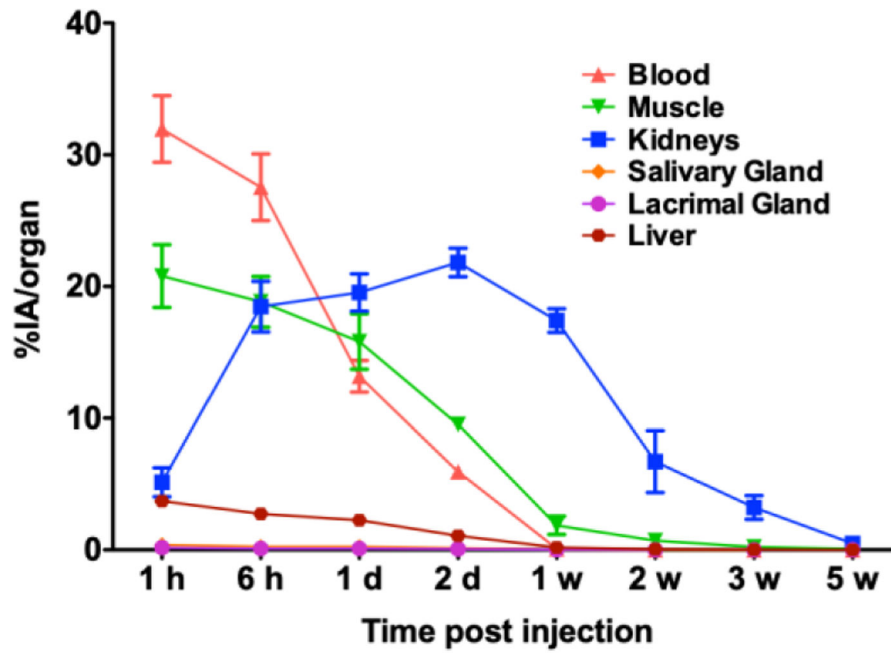
Figure 2.
Tumor volume and survival curve for dose optimization study. **a** Tumor growth over time for control groups; **b** Tumor growth over time for treatment groups; **c** Enlarged view of tumor growth over time for treatment groups in the first 28 days; **d** Kaplan-Meier survival curve for all groups.

Figure 3.
SPECT/CT imaging of selected animals over treatment period. Top row, representative mouse from CTT1403 group. Bottom row, representative mouse from CTT1751 group. Right side, SPECT signal scale from 10 to 100 (counts per second). White arrow showing tumor, Red outline showing phantom dose.

Figure 4.
SPECT/CT imaging quantification. **a** CTT1403 organ uptake; **b** CTT1751 organ uptake; **c**
Tumor:background ratios based on mean signal value.

Figure 5.
Decay-corrected time-activity curves of CTT1403 in key PSMA+ (kidneys) and non-target tissues (blood, muscle, salivary gland, lacrimal gland, liver) in rats at 1 h, 6 h, 1 d, 2 d, 1 w, 2 w, 3 w and 5 w.

Table 1

Summary table of pairwise log-rank tests of survival from tumor implantation (Fig. 2d), stratified by cohort.

Group 1	Group 2	log-rank test p-value	adjusted p-value[a]
Merged control[b]	CTT1403×1[c]	0.021	0.095
Merged control	CTT1403×2[c]	<0.001	<0.001
Merged control	CTT1403×3[c]	<0.001	<0.001
CTT1403×1	CTT1403×2	0.007	0.037
CTT1403×1	CTT1403×3	0.006	0.031
CTT1403×2	CTT1403×3	0.961	0.999

[a] multiple pairwise comparisons adjustment by Tukey's studentized range test.[35]

[b] N = 18 (Saline, [^{175}Lu]CTT1403, CTT1751)

[c] N = 6 each

Table 2.

Estimated Organ Doses (mSv/MBq) from integration of human time-activity-curves for OLINDA/EXM 1.0 source organs (biodistribution from 30 normal Sprague Dawley male rats).

Target Organ	Beta	Photon	Total	EDE Cont.	ED Cont.
Adrenals	1.02E-01	1.75E-02	1.19E-01	7.16E-03	2.98E-04
Brain	1.11E-02	1.65E-03	1.27E-02	0.00E+00	3.19E-05
Breasts	1.48E-02	2.53E-03	1.73E-02	2.60E-03	8.67E-04
Gallbladder Wall	1.48E-02	1.12E-02	2.60E-02	0.00E+00	0.00E+00
LLI Wall	4.06E-02	5.09E-03	4.57E-02	0.00E+00	5.49E-03
Small Intestine	3.97E-02	7.91E-03	4.76E-02	0.00E+00	1.19E-04
Stomach Wall	2.10E-02	7.98E-03	2.90E-02	0.00E+00	3.48E-03
ULI Wall	2.79E-02	7.72E-03	3.57E-02	0.00E+00	8.91E-05
Heart Wall	7.53E-02	5.98E-03	8.13E-02	4.88E-03	0.00E+00
Kidneys	5.09E+00	9.36E-02	5.18E+00	3.11E-01	1.30E-01
Liver	4.06E-02	9.20E-03	4.98E-02	0.00E+00	2.49E-03
Lungs	9.81E-02	5.15E-03	1.03E-01	1.24E-02	1.24E-02
Muscle	3.03E-02	4.61E-03	3.49E-02	0.00E+00	8.73E-05
Pancreas	7.19E-02	1.36E-02	8.55E-02	5.13E-03	2.14E-04
Red Marrow	4.84E-02	6.36E-03	5.48E-02	6.57E-03	6.57E-03
Osteogenic Cells	1.68E-01	8.53E-03	1.77E-01	5.31E-03	1.77E-03
Skin	1.48E-02	2.42E-03	1.72E-02	0.00E+00	1.72E-04
Spleen	5.74E-02	1.60E-02	7.33E-02	4.40E-03	1.83E-04
Testes	8.89E-02	3.38E-03	9.22E-02	2.31E-02	1.84E-02
Thymus	5.93E-02	3.99E-03	6.33E-02	0.00E+00	1.58E-04
Thyroid	9.34E-02	3.70E-03	9.71E-02	2.91E-03	4.86E-03
Urinary Bladder Wall	4.37E-02	4.46E-03	4.82E-02	0.00E+00	2.41E-03
Total Body	5.39E-02	5.29E-03	5.92E-02	0.00E+00	0.00E+00
Effective Dose Equivalent (mSv/MBq)				3.85E-01	
Effective Dose (mSv/MBq)					1.90E-01
Prostate			5.53E-02		
Lacrimal Gland			1.19E-01		
Salivary Gland			8.56E-02		